Plasma Response to Resonant Perturbations at Tokamak Edge

André Carlos Fraile Júnior, Marisa Roberto & Iberê Luiz Caldas

Brazilian Journal of Physics

ISSN 0103-9733

Braz J Phys
DOI 10.1007/s13538-018-0584-6

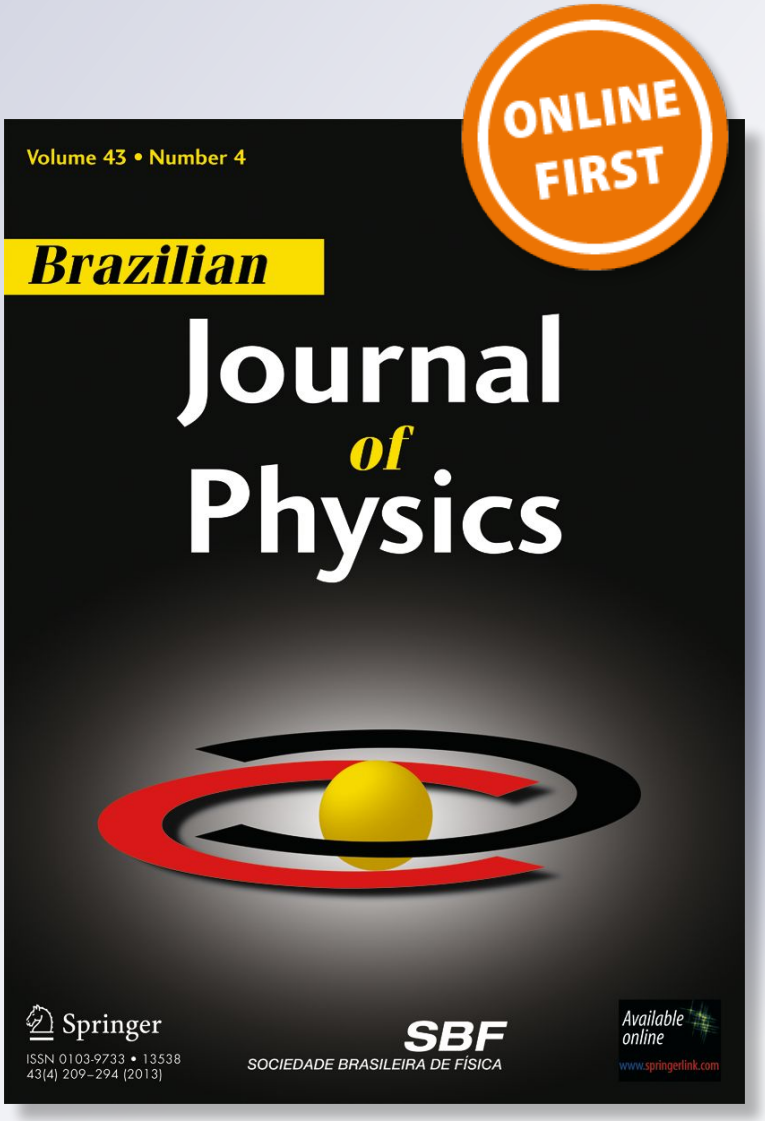

Springer

Your article is protected by copyright and all rights are held exclusively by Sociedade Brasileira de Física. This e-offprint is for personal use only and shall not be self-archived in electronic repositories. If you wish to self-archive your article, please use the accepted manuscript version for posting on your own website. You may further deposit the accepted manuscript version in any repository, provided it is only made publicly available 12 months after official publication or later and provided acknowledgement is given to the original source of publication and a link is inserted to the published article on Springer's website. The link must be accompanied by the following text: "The final publication is available at link.springer.com”.

Springer

Author's personal copy

Brazilian Journal of Physics
https://doi.org/10.1007/s13538-018-0584-6

GENERAL AND APPLIED PHYSICS

Plasma Response to Resonant Perturbations at Tokamak Edge

André Carlos Fraile Júnior [1,2] · Marisa Roberto [1] · Iberê Luiz Caldas [3]

Received: 12 April 2018 /
© Sociedade Brasileira de Física 2018

Abstract

In certain circumstances, plasma response suppresses magnetic islands expected at perturbed resonant magnetic surfaces. We investigate the plasma response to the resonant magnetic perturbations in a large aspect ratio tokamak perturbed by external resonant helical windings, considering polar toroidal coordinates for which analytical toroidal equilibrium solutions and perturbing fields are available. We apply an empirical approach to mimic the plasma screening effects by introducing presumed plasma current sheets on the resonance surfaces to cancel the RMP effects. Numerical examples show the effect of plasma response reducing magnetic islands at the plasma edge and also regularizing field lines around the resonant surface. The distribution of connection lengths along the plasma cross section indicates that the plasma response increases the connection lengths since more toroidal turns are performed until a field line reaches the tokamak wall.

Keywords Plasma response · Resonant magnetic perturbation (RMP) · Tokamak

1 Introduction

One of the main challenges in designing tokamak components is related to the heat and particles fluxes on the tokamak wall, since high-temperature particles collide with surfaces and plasma disruptions impose mechanical loads to its structure [1]. Sets of coils placed around the tokamak external wall, such as the ergodic magnetic limiter (EML) [2–5] and resonant helical windings [6–9], have been widely studied due to the generation of resonant magnetic perturbations capable of creating a chaotic layer near the plasma edge, reducing the tokamak wall erosion [10, 11].

An example of these external coils, resonant helical windings conduct currents with the same helicity as one of the plasma equilibrium magnetic flux surfaces, located near the plasma edge, creating resonant magnetic perturbations (RMP) that generate a chaotic layer around the resonant surface [4]. This RMP affects the magnetic field and the plasma itself, whose response to perturbations has been the subject of investigations [12–14]. Although a complete analysis of plasma response and its contribution to the total magnetic field would require a complex study of resistive magnetohydrodynamics [15], some models have been developed to simulate the plasma response and they provide an effective way of evaluating its effect on magnetic flux surfaces and particle distribution.

Comparisons between vacuum calculations without and with plasma response have shown that helical current sheets mitigate magnetic islands, simulating the effects of plasma response in experiments where the width of the stochastic layer is smaller than the one predicted by vacuum calculations [16]. One model of plasma response considers screening plasma reaction on the main resonant surfaces [12]. In [17], we have applied the model introduced in [12] for a large aspect ratio tokamak perturbed by resonant helical windings. The equilibrium magnetic field was calculated for a periodical cylinder with small corrections in the toroidal field. In the applied model, the plasma response to a perturbation generated by a pair of helical windings was modeled as an additional RMP associated to a current sheet located at a resonant surface with the condition that the radial component of the total magnetic field vanished at this surface. This condition of perturbation screening mimics the complete mitigation of magnetic islands around a chosen resonant surface [12, 13], which is justified when a strong pressure gradient suppresses resonant modes at

✉ Marisa Roberto
marisar@ita.br

[1] Departamento de Física, Instituto Tecnológico de Aeronáutica, São José dos Campos, Brazil

[2] Divisão de Aerotermodinâmica e Hipersônica, Instituto de Estudos Avançados, São José dos Campos, Brazil

[3] Departamento de Física Aplicada, Instituto de Física, Universidade de São Paulo, São Paulo, Brazil

Published online: 12 June 2018

Author's personal copy

the plasma edge [12]. Although several screening surfaces could be considered, the results confirm that a single surface is enough to significantly account for the size of footprints and also the beginning of open field line region for COMPASS and JET [13]. This phenomenological approach is not ideal, since it does not address the deep cause of island suppression. Nevertheless, it could be acceptable, in view of the challenging feature of this topic.

Here, we extend the previous analysis reported in [17] by considering analytical plasma equilibria obtained for large aspect ratio tokamaks in terms of polar toroidal coordinates introduced to describe toroidal magnetic surfaces presenting a Shafranov shift toward the exterior equatorial region [18]. The considered external perturbation is due to currents in pairs of helical windings presented in [17] and the screening model is that introduced in [12]. Based on the obtained analytical magnetic field components, the field line equations have been solved numerically and the Poincaré maps associated to a plasma cross section without and with plasma response are obtained. They show the reduction of magnetic islands and the regularization of field lines around the resonant surface when the plasma response is taken into account, which is an effect also observed in earlier numerical studies [12, 13, 19–22]. The analysis of connection lengths, which are related to the number of toroidal turns a magnetic field line performs from an initial condition until it reaches the wall, shows that not only the perturbation is completely screened at the resonant surface, but also field lines perform more toroidal turns from a set of initial conditions chosen near the plasma edge. The obtained equilibrium and perturbing field analytical expressions can be useful to investigate the dynamics of the reduction of magnetic islands and the less pronounced chaotic pattern.

Section 2 presents the magnetohydrodynamical equilibrium associated to a large aspect ratio tokamak. In section 3, the magnetic field produced by helical windings is presented. The plasma response associated to this RMP is calculated in section 4. Section 5 presents the numerical results in Poincaré maps obtained with this model. Section 6 shows results concerning the effects of plasma response on connection lengths. The conclusions are presented in section 7.

2 Magnetohydrodynamical Equilibrium

The static plasma equilibrium is described by the solution of the following set of equations [4].

$$\begin{cases} \vec{J} \times \vec{B}_0 = \nabla p \\ \nabla \times \vec{B}_0 = \mu_0 \vec{J} \\ \nabla \cdot \vec{B}_0 = 0 \end{cases}, \tag{1}$$

where p is the pressure, $\vec{B}_0$ is the magnetic field, $\vec{J}$ is the current density, and μ_0 is the vacuum permeability. The solution of these equations can be expressed as a function of the poloidal magnetic flux ψ_p. In this work, we choose the following density profile along the plasma cross section [4].

$$J_{\varphi_t}(r_t) = \frac{I_p R_0'}{\pi a^2}(\gamma+1)\left[1-\left(\frac{r_t}{a}\right)^2\right]^{\gamma}, \tag{2}$$

where $\gamma = 3$ is a constant parameter, I_p is the plasma current, a is the plasma column radius, and R_0' is the distance of the magnetic axis to the tokamak center. The current profile shown in (2) is presented in polar toroidal coordinates (r_t, θ_t, φ_t) [18], used to obtain analytically the equilibrium poloidal magnetic flux ψ_p from the Grad-Shafranov equation. The solution is valid for large aspect ratio tokamaks, and the surfaces with constant ψ_p are not concentric in the plasma cross section, displaying a Shafranov shift [18].

The current profiles shown in Eq. (2) and the set of Eq. (1) provide the function ψ_p and, consequently, the equilibrium magnetic field is given [4]:

$$\vec{B}_0 \cong \frac{\mu_0 I_p}{2\pi r_t^2}\left[1-\left(1-\frac{r_t^2}{a^2}\right)^{\gamma+1}\right]\vec{e}_{\theta_t} + \frac{\mu_0 I_e}{2\pi R_0'^2\left(1-2r_t\cos\theta_t/R_0'\right)}\vec{e}_{\varphi_t}, \tag{3}$$

where I_e is the external current generating the toroidal magnetic field.

The safety factor associated to this equilibrium field is expressed as [4]

$$q(r_t) = \frac{1}{2\pi}\int_0^{2\pi}\frac{B_0^{\varphi_t}}{B_0^{\theta_t}}d\varphi_t = q_c(r_t)\left(1-4r_t^2/R_0'^2\right)^{-1/2}, \tag{4}$$

where $q_c(r_t) = I_e r_t^2/\left(I_p R_0'^2\right)\left[1-\left(1-r_t^2/a^2\right)^{\gamma+1}\right]^{-1}$ represents the safety factor for a cylindrical plasma.

For numerical application, we use the TCABR tokamak parameters [23]. Thus, Fig. 1 presents the safety factor profile along the plasma cross section for the TCABR tokamak with parameters: external current $I_e = 4$MA, plasma radius a = 0.18m, tokamak minor radius $b = 0.22$ m, major radius R_0 = 0.61m, and plasma current $I_p = 50$ kA. In the same figure, the radial position $r_0/a \cong 0.83$ associated to $q(r_0) = 5$ is represented, since all calculations and analyses in the following sections occur around this region.

3 Resonant Helical Windings

In this work, resonant magnetic perturbations are included in order to create a layer of chaotic field lines near the tokamak

Author's personal copy

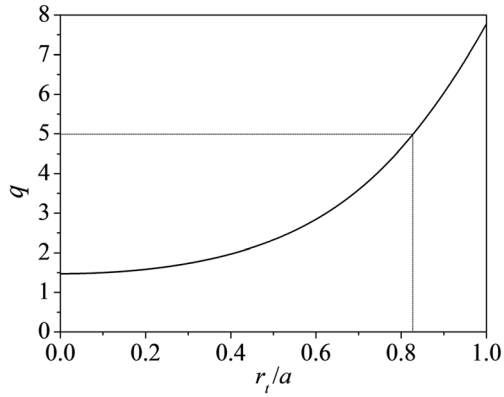

Fig. 1 Safety factor profile along the plasma cross section, emphasizing the radial coordinate associated to $q = 5$

wall. Two resonant helical windings conducting current I_p in opposing directions are located on the tokamak external wall separated by 180°, $r_t = b_t$, with poloidal mode number m_0 and toroidal mode number n_0. The variable $u_h = m_0\theta_t - n_0\varphi_t$ is used to define the winding law as the set of points with $u_h =$ constant [4]. The helical windings with mode numbers (m_0, n_0) are resonant to surface $r_t = r_0$, which means they both have the same helicity of the equilibrium magnetic field at this surface.

The current density associated to the external helical windings is expressed as [4]

$$\vec{J}_h = \frac{I_h}{R_0' r_t}\delta(r_t - b_t)[\delta(u_h - 0) - \delta(u_h - \pi)]\vec{e}_{hel}, \tag{5}$$

where $\vec{e}_{hel}$ is associated to the helix direction [4].

The magnetic field due to the helical windings is expressed as $\vec{B}_h(r_t, \theta_t, \varphi_t) = \nabla\phi_h(r_t, \theta_t, \varphi_t)$, which must satisfy $\nabla\cdot\vec{B}_h(r_t, \theta_t, \varphi_t) = 0$, resulting in the equation [4]

$$\nabla^2\phi_h(r_t, \theta_t, \varphi_t) = 0. \tag{6}$$

Considering a large aspect ratio tokamak, for a region $r_t \leq b_t$, the solution of Eq. (6) can be approximated to [4]

$$\phi_h(r_t, \theta_t, \varphi_t) = -\frac{\mu_0 I_h}{i\pi}\sum_{N=1}^{\infty}\frac{1}{N}\left(\frac{r_t}{b_t}\right)^{Nm_0} e^{iN(m_0\theta_t - n_0\varphi_t)}. \tag{7}$$

The scalar magnetic potential shown in Eq. (7) provides the magnetic field components due to the helical windings

$$B_{h,r_t}(r_t, \theta_t, \varphi_t) = -\frac{\mu_0 I_h m_0}{i\pi b_t}\sum_{N=1}^{\infty}\left(\frac{r_t}{b_t}\right)^{Nm_0-1} e^{iN(m_0\theta_t - n_0\varphi_t)}, \tag{8}$$

$$B_{h,\theta_t}(r_t, \theta_t, \varphi_t) = -\frac{\mu_0 I_h m_0}{\pi}\sum_{N=1}^{\infty}\left(\frac{r_t}{b_t}\right)^{Nm_0} e^{iN(m_0\theta_t - n_0\varphi_t)}, \tag{9}$$

and

$$B_{h,\varphi_t}(r_t, \theta_t, \varphi_t) = \frac{\mu_0 I_h n_0}{\pi}\sum_{N=1}^{\infty}\left(\frac{r_t}{b_t}\right)^{Nm_0} e^{iN(m_0\theta_t - n_0\varphi_t)}. \tag{10}$$

These equations will be used in the numerical applications of section 5.

4 Plasma Response

In order to mimic the plasma response, we include another RMP due to a current sheet at the surface $r_t = r_0$ and calculate its contribution to the total magnetic field, under the condition that its radial component vanishes at $r_t = r_0$ [12]. Although several screening surfaces could be considered as shown in experiments in JET and COMPASS [13], this work analyzes the effect of a single surface on the field line distribution along a plasma cross section. Early studies have shown that a single screening surface can already modify significantly the footprint size as well as the beginning of the open field line region or the field line escaping [13].

The current density associated to this single current sheet is defined as

$$\vec{J}_{pr} = \frac{j}{R_0' r_t}\delta(r_t - r_0)\vec{e}_{hel}, \tag{11}$$

where

$$j = \sum_{N=1}^{+\infty} j_N e^{iN(m_0\theta_t - n_0\varphi_t)}. \tag{12}$$

The magnitude of the current is obtained from the plasma response condition, which specifies that the radial component of the total magnetic field is 0 at $r_t = r_0$, which means that $\left(\vec{B}_0 + \vec{B}_h + \vec{B}_{pr}\right)\cdot\nabla r_t = 0$, where $\vec{B}_h$ is the magnetic field associated to the helical windings and $\vec{B}_{pr}$ is associated to the current sheet.

In order to obtain $\vec{B}_{pr}$, the same procedure detailed in the previous section is applied here to calculate the magnetic field due to a conducting surface at $r_t = r_0$: since $\vec{B}_{pr} = \nabla\phi_{pr}$ for $r_t \neq r_0$ and $\nabla\cdot\vec{B}_{pr} = 0$, the equation $\nabla^2\phi_{pr}(r_t, \theta_t, \varphi_t) = 0$ is solved in polar toroidal coordinates. The general solution associated to a large aspect ratio tokamak is

$$\phi_{pr}(r_t, \theta_t, \varphi_t) = \begin{cases} \sum_{N=-\infty}^{\infty} C_N^i (r_t/b_t)^{|Nm_0|} e^{iN(m_0\theta_t - n_0\varphi_t)}, \text{ if } r_t \leq r_0 \\ \sum_{N=-\infty}^{\infty} C_N^e (r_t/b_t)^{-|Nm_0|} e^{iN(m_0\theta_t - n_0\varphi_t)}, \text{ if } r_t > r_0 \end{cases}, \tag{13}$$

Author's personal copy

where C_N^i and C_N^e are constants calculated from boundary conditions.

The magnetic field components associated to the scalar magnetic potential shown in Eq. (13) are obtained when the plasma response condition, $\left(\vec{B}_0 + \vec{B}_h + \vec{B}_{pr}\right) \cdot \nabla r_t = 0$, is taken into account:

$$B_{pr,r_t}(r_t,\theta_t,\varphi_t) = \begin{cases} \mu_0 \sum_{N=1}^{\infty} \frac{I_h m_0}{i\pi r_0} \left(\frac{r_0}{b_t}\right)^{Nm_0} \left(\frac{r_t}{r_0}\right)^{Nm_0-1} e^{iN(m_0\theta_t - n_0\varphi_t)}, \text{ if } r_t \le r_0 \\ \mu_0 \sum_{N=1}^{\infty} \frac{I_h m_0}{i\pi r_0} \left(\frac{r_0}{b_t}\right)^{Nm_0} \left(\frac{r_t}{r_0}\right)^{-Nm_0-1} e^{iN(m_0\theta_t - n_0\varphi_t)}, \text{ if } r_t > r_0 \end{cases}, \tag{14}$$

$$B_{pr,\theta_t}(r_t,\theta_t,\varphi_t) = \begin{cases} \mu_0 \sum_{N=1}^{\infty} \frac{I_h m_0}{\pi} \left(\frac{r_t}{b_t}\right)^{Nm_0} e^{iN(m_0\theta_t - n_0\varphi_t)}, \text{ if } r_t < r_0 \\ -\mu_0 \sum_{N=1}^{\infty} \frac{I_h m_0}{\pi} \left(\frac{b_t r_t}{r_0^2}\right)^{-Nm_0} e^{iN(m_0\theta_t - n_0\varphi_t)}, \text{ if } r_t > r_0 \end{cases}, \tag{15}$$

and

$$B_{pr,\varphi_t}(r_t,\theta_t,\varphi_t) = \begin{cases} -\mu_0 \sum_{N=1}^{\infty} \frac{I_h n_0}{\pi} \left(\frac{r_t}{b_t}\right)^{Nm_0} e^{iN(m_0\theta_t - n_0\varphi_t)}, \text{ if } r_t < r_0 \\ \mu_0 \sum_{N=1}^{\infty} \frac{I_h n_0}{\pi} \left(\frac{b_t r_t}{r_0^2}\right)^{-Nm_0} e^{iN(m_0\theta_t - n_0\varphi_t)}, \text{ if } r_t > r_0 \end{cases}. \tag{16}$$

These expressions obtained for the plasma response will be applied in the next section.

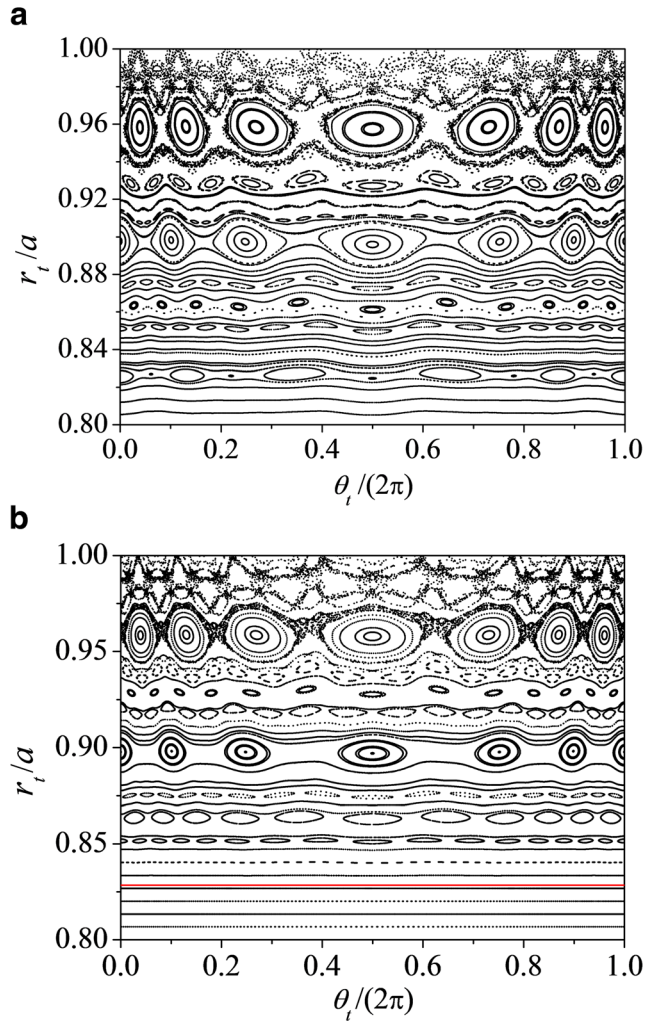

Fig. 2 Poincaré maps for perturbation parameter $I_h = 0.05\ \%\ I_p$ **a** without plasma response and **b** with plasma response. In **b**, the red horizontal line is associated to the surface $r_t = r_0$

5 Numerical Results

Considering the total magnetic field $\vec{B} = \vec{B}_0 + \vec{B}_h + \vec{B}_{pr}$ and an infinitesimal displacement $d\vec{l}$ along the field lines, the equation $\vec{B} \times d\vec{l} = \vec{0}$ is integrated numerically in order to obtain the Poincaré map associated to the set of points (r_t,θ_t) when the cross section $\varphi_t = 0$ is intercepted by a field line. The helical windings are resonant to the mode $(m_0, n_0) = (5, 1)$, which is associated to surface $r_0/a \cong 0.83$. Poincaré maps with perturbation parameters $I_h = 0.05\ \%\ I_p$ and $I_h = 0.5\ \%\ I_p$ are shown in Figs. 2 and 3 for a set of initial conditions. We emphasized that, in this coordinate system, in which toroidal effects affect all magnetic field lines, the perturbation current is much lower than considered in our previous paper [17].

Without taking into account the effect of plasma response, Fig. 2a shows the formation of magnetic islands around the perturbed surface $r_0/a \cong 0.83$ due to the (5, 1) helical windings. We observe the $m = 5$ island chain, at the resonant invariant line at $r_t = r_0$, and other secondary island chains at the plasma edge due to the toroidal geometry. When the plasma response is taken into account, as represented in Eqs. (14) to (16), the islands located at $r_t = r_0$ vanish due to the plasma response condition, $\left(\vec{B}_0 + \vec{B}_h + \vec{B}_{pr}\right) \cdot \nabla r_t = 0$. Thus, in Fig. 2b, a red horizontal invariant line represents the magnetic surface intersection that is positioned at $r_t = r_0$ as a result of a complete mitigation of magnetic islands at the resonant surface. Field lines around $r_t = r_0$ are regularized, agreeing with results from computational codes [12, 13, 19–22]. In our previous work, as a consequence of the simplified geometry associated to a cylindrical plasma, perturbation currents larger than $5\%I_p$ were applied to the helical windings in order to observe a thick chaotic region near the plasma edge [17]. In this work, however, due to the toroidal geometry, a perturbation current of $0.05\%I_p$ applied to resonant helical windings is enough to produce chaotic regions, as indicated in Fig. 2a and also corroborated by similar results in reference [4].

Author's personal copy

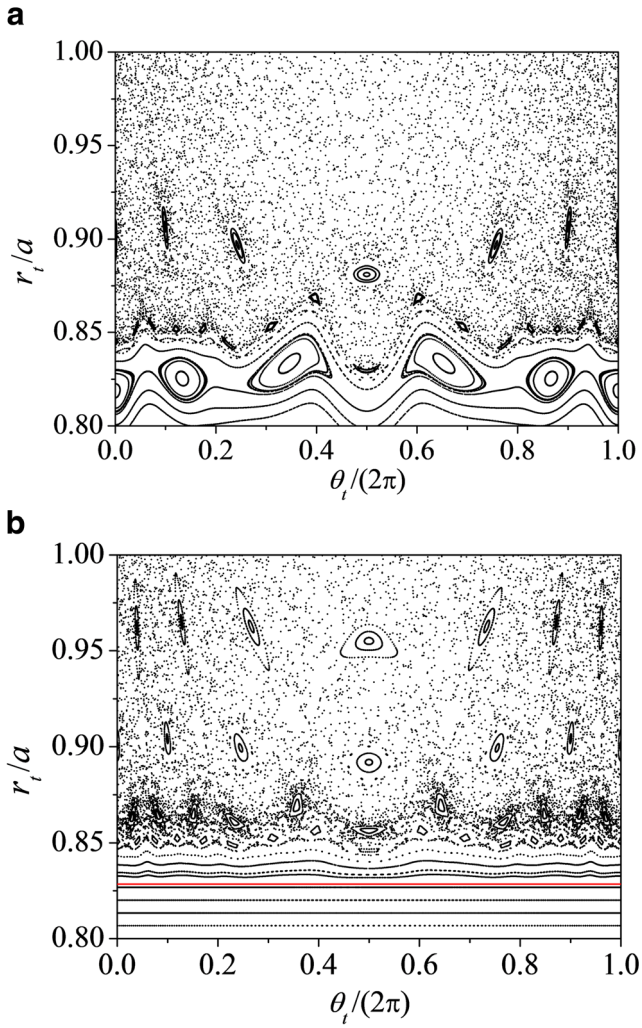

Fig. 3 Poincaré maps for perturbation parameter $I_h = 0.5\ \%\ I_p$ **a** without plasma response and **b** with plasma response. In **b**, the red horizontal line is associated to the surface $r_t = r_0$

Figure 3 shows that increasing the perturbation parameter from $0.05\%I_p$ to $0.5\%I_p$ has the effect of amplifying the layer of chaotic field lines near the plasma edge while most magnetic islands are destroyed. On the other hand, as presented in Figs. 2b and 3b, when the plasma response effect is considered on the total magnetic field, the chaotic layer is restricted to $r_t/a > 0.83$ and the perturbation is screened at surface $r_0/a \cong 0.83$. In Fig. 3a, the island chain associated to mode $(m, n) = (7, 1)$ is not visible, while in Fig. 3b, when the plasma response is considered, the main chains associated to modes (6, 1) and (7, 1) remain visible even with this high perturbation current. Although the chaos is predominant in the region $r_t > 0.85$, we also note a regularization effect and the transport barrier, as observed in Fig. 3b, created by imposing $\left(\vec{B}_0 + \vec{B}_h + \vec{B}_{pr}\right) \cdot \nabla r_t = 0$ at $r_t = r_0$, which is similar to a robust torus, as reported by references [24, 25].

6 Connection Lengths

In order to evaluate the transport of particles to the tokamak wall, this section presents the effects of plasma response on the connection length distribution in the plasma cross section $\varphi_t = 0$. For each initial condition located in the section delimited by $0.8 \le r_t/a \le 1.0$ and $0 \le \theta_t/(2\pi) \le 1.0$, the number of toroidal turns that a field line performs until reaching the tokamak wall is defined as the connection length associated to this initial condition. Figure 4 presents the distribution of connection lengths at cross section $\varphi_t = 0$ for perturbation parameter $0.5\%I_p$. We have chosen a higher perturbation case to show easily how connection lengths are affected by plasma response. With low perturbation current, the most of magnetic field lines would be trapped for 1000 toroidal turns.

Figure 4a shows that trapped magnetic field lines are located at magnetic islands and the chaotic layer is characterized by field lines escaping with a wide range of toroidal turns: while field lines initially located near the plasma edge escape with less than 50 toroidal turns, some lines close to the last magnetic surface require more turns to reach the tokamak wall. On the other hand, as presented in Fig. 4b, when the plasma response is considered, a transport barrier is created at the

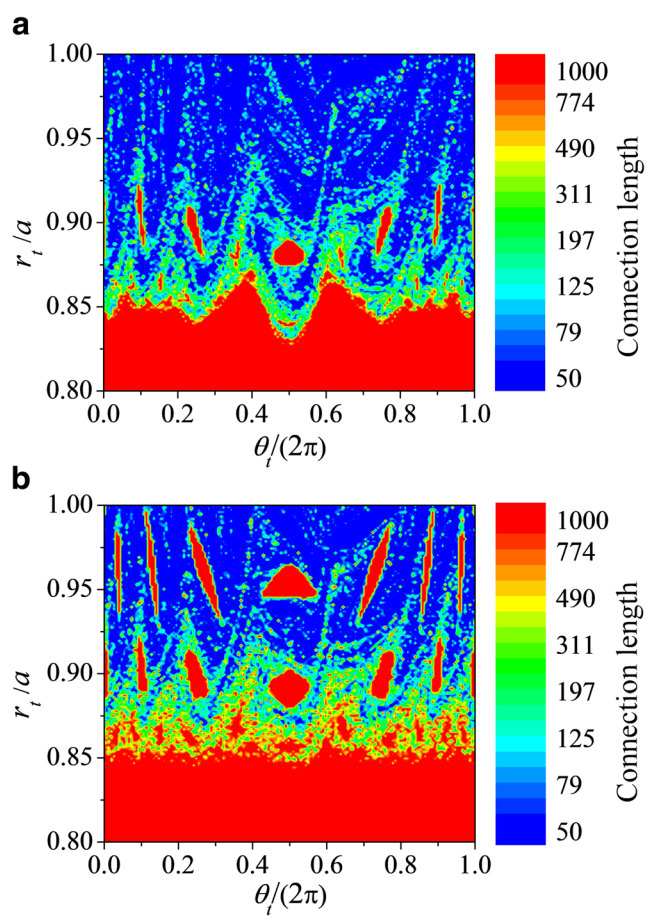

Fig. 4 Connection lengths for $I_h = 0.5\%I_p$ **a** without plasma response and **b** with plasma response

Author's personal copy

resonant surface $r_0/a = 0.83$, screening the helical winding perturbation and preventing any lines inside this surface from reaching the tokamak wall, while the magnetic islands around $r_0/a = 0.83$ also shrink as previously discussed in section 5. Besides, near the plasma edge, field lines initially located in magnetic islands associated to islands (7, 1) are trapped when the plasma response is considered, while in Fig. 4a they escape with few toroidal turns. The transport barrier at $r_0/a = 0.83$ reduces the island widths in the external rational surfaces (where the safety factor q is rational) and, consequently, the chaotic region at the plasma edge. This is a coupling effect due to the toroidal geometry, i.e., the considered perturbing current density in the resonant surface acts also on the other rational surfaces reducing the island widths.

In order to evaluate the effect of plasma response on the number of trapped field lines, Fig. 5 presents the connection lengths associated to a set of initial conditions along $\theta_t/(2\pi) = 0.25$ for perturbation parameter $0.5\% I_p$.

Figure 5a shows that a small plateau is located around the magnetic island associated to islands (5, 1) and (6, 1), while the remaining field lines escape with different values of toroidal turns. Figure 5b, with plasma response, shows that all field lines for initial conditions located in $r_t < r_0$ are trapped in invariant lines observed in Fig. 4b. A plateau is also observed around $r_t/a = 0.96$ as an effect of plasma response, which is related to island chains that were observed in Fig. 3b.

The statistical analysis of connection lengths distribution in Fig. 5a shows that, without plasma response, approximately 30% of the field lines perform 900 or more toroidal turns, while 50% escape with less than 100 toroidal turns. When the plasma response is taken into account (Fig. 5b), approximately 50% of the field lines perform 900 or more toroidal turns, corroborating that the plasma response increases the amount of field lines trapped on the plasma, while only 30% escape with less than 100 turns. We have seen that the extension of chaotic layer is reduced when the plasma response is taken into account considering the perturbation solo on (5, 1) surface. As we already mentioned, a single perturbed surface is enough to significantly account for the size of footprints for tokamaks such as COMPASS and JET [13].

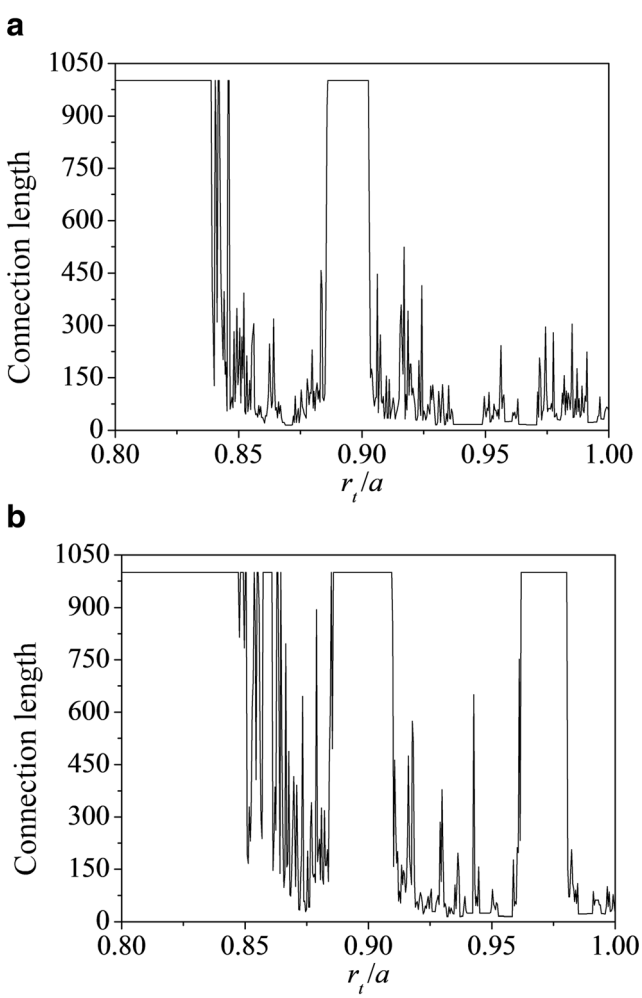

Fig. 5 Connection lengths for magnetic field lines located on $\theta_t/(2\pi) = 0.25$ and perturbation parameter $I_h = 0.5\% I_p$ **a** without plasma response; **b** with plasma response

7 Conclusions

In this work, analytical toroidal plasma equilibrium has been described by polar toroidal coordinates. In terms of these coordinates, the external resonant perturbation and the plasma response were also calculated. The resonant magnetic perturbation was created by helical windings located at the tokamak external wall, while the plasma response was mimicked by a current sheet located at the perturbed surface with the additional condition that the radial component of the total magnetic field is eliminated at the perturbed surface, reducing the chaotic region in phase space.

The field line equation was integrated and showed that the addition of plasma response to vacuum calculations has the effect of shrinking magnetic islands and also regularizes field lines around the resonant surface, which was also observed in earlier studies with numerical codes. The condition of screening of perturbations in the resonant surface showed that a transport barrier similar to a robust torus is created at this surface.

Although increasing the perturbation current has caused a larger chaotic layer to appear near the plasma edge, the analysis of connection lengths, calculated as the number of toroidal turns performed by field lines from an initial condition until the wall is reached, showed that the plasma response increases the number of trapped field lines near the edge while all lines inside the perturbed surface are prevented from reaching the tokamak wall.

Author's personal copy

Funding Information The authors thank the financial support from São Paulo Research Foundation (FAPESP, Brazil) under grants Nos 2015/16471-8 and 2011/19296-1, CNPq (Brazil) under grant No 446905/2014-3 and CAPES (Brazil).

References

1. R. Parker, G. Janeschitz, H.D. Pacher, D. Post, S. Chiocchio, G. Federici, P. Ladd, J. Nucl. Mater. **1**, 241–243 (1997)
2. P. Ghendrih, A. Grosman, H. Capes, Plasma Phys. Control. Fusion **38**, 1653–1724 (1996)
3. F. Karger, K. Lackner, Phys. Lett. A **61**, 385–387 (1977)
4. E.C. da Silva, I.L. Caldas, R.L. Viana, IEEE Trans. Plasma Sci. **29**, 617–631 (2001)
5. M. Roberto, E.C. da Silva, I.L. Caldas, R.L. Viana, Phys. Plasmas **11**, 214–225 (2004)
6. S.S. Abdullaev, *Magnetic Stochasticity in Magnetically Confined Fusion Plasmas*, 1st edn. (Springer, Berlin, 2014), pp. 227–262
7. M. Lehnen, S.S. Abdullaev, W. Biel, S. Brezinsek, K.H. Finken, D. Harting, M. von Hellermann, M. Jakubowski, R. Jaspers, M. Kobayashi, H.R. Koslowski, A. Krämer-Flecken, G. Matsunaga, A. Pospieszczyk, D. Reiter, T. Van Rompuy, U. Samm, O. Schmitz, G. Sergienko, B. Unterberg, R. Wolf, O. Zimmermann, T.E.X.T.O.R. Team, J. Nucl. Mater. **337-339**, 171–175 (2005)
8. K.H. Finken, B. Unterberg, Y. Xu, S.S. Abdullaev, M. Jakubowski, M. Lehnen, M.F.M. de Bock, S. Bozhenkov, S. Brezinsek, C. Busch, I.G.J. Classen, J.W. Coenen, D. Harting, M. von Hellermann, S. Jachmich, R.J.E. Jaspers, Y. Kikuchi, A. Krämer-Flecken, Y. Liang, M. Mitri, P. Peleman, A. Pospieszczyk, D. Reiser, D. Reiter, U. Samm, D. Schega, O. Schmitz, S. Soldatov, M. Van Schoor, M. Vergote, R.R. Weynants, R. Wolf, O. Zimmermann, T.E.X.T.O.R. Team, Nucl. Fusion **47**, 522–534 (2007)
9. O. Schmitz, T.E. Evans, M.E. Fenstermacher, E.A. Unterberg, M.E. Austin, B.D. Bray, N.H. Brooks, H. Frerichs, M. Groth, M.W. Jakubowski, C.J. Lasnier, M. Lehnen, A.W. Leonard, S. Mordijck, R.A. Moyer, T.H. Osborne, D. Reiter, U. Samm, M.J. Schaffer, B. Unterberg, W.P. West, Phys. Rev. Lett. **103**, 165005 (2009)
10. T.E. Evans, Plasma Phys. Control. Fusion **57**, 123001 (2015)
11. E.C. da Silva, I.L. Caldas, R.L. Viana, M.A.F. Sanjuán, Phys. Plasmas **9**, 4917–4928 (2002)
12. P. Cahyna, E. Nardon, J. Nucl. Mater. **415**, S927–S931 (2011)
13. H. Frerichs, D. Reiter, O. Schmitz, P. Cahyna, T.E. Evans, Y. Feng, E. Nardon, Phys. Plasmas **19**, 052507 (2012)
14. F.L. Waelbroeck, I. Joseph, E. Nardon, M. Bécoulet, R. Fitzpatrick, Nucl. Fusion **52**, 074004 (2012)
15. D. Ciro, T.E. Evans, I.L. Caldas, Nucl. Fusion **57**, 016017 (2017)
16. P. Cahyna, M. Peterka, A. Kirk, A. Thornton, J. Harrison, D. Muir, R. Panek, J. Nucl. Mater. **438**, S326–S329 (2013)
17. A.C. Fraile Jr., M. Roberto, I.L. Caldas, C.G.L. Martins, IEEE Trans. Plasma Sci. **45**, 11 (2017)
18. M.Y. Kucinski, I.L. Caldas, L.H.A. Monteiro, V. Okano, Aust. J. Plant Physiol. **44**, 303 (1990)
19. Y. Liu, C.J. Ham, A. Kirk, L. Li, A. Loarte, D.A. Ryan, Y. Sun, W. Suttrop, X. Yang, L. Zhou, Plasma Phys. Control. Fusion **58**, 114005 (2016)
20. A. Yueqiang Liu, Y.S. Kirk, Phys. Plasmas **20**, 042503 (2013)
21. F. Orain, M. Hölzl, E. Viezzer, M. Dunne, M. Bécoulet, P. Cahyna, G.T.A. Huijsmans, J. Morales, M. Willensdorfer, W. Suttrop, A. Kirk, S. Pamela, S. Günter, K. Lackner, E. Strumberger, A. Lessig, Nucl. Fusion **57**, 022013 (2017)
22. E. Nardon, M. Bécoulet, G. Huysmans, O. Czarny, Phys. Plasmas **14**, 092501 (2007)
23. E.C. da Silva, I.L. Caldas, R.L. Viana, Braz. J. Phys. **32**, 39 (2002)
24. R. Egydio de Carvalho, C.G.L. Martins, G.M. Favaro, Braz. J. Phys. **39**, 606–614 (2009)
25. R. Egydio de Carvalho, G.M. Favaro, Physica A **350**, 173–182 (2005)